UNIVERSITY OF CALIFORNIA, SAN DIEGO

Design of a Steady State Thermal Conductivity Measurement Device for CNT RET Polymer Composites.

A Thesis submitted in partial satisfaction of the requirements

for the degree Master of Science

in

Mechanical Engineering

by

Brian Ming Louie

Committee in charge:

Professor Prabhakar R. Bandaru, Chair
Professor Renkun Chen
Professor Sungho Jin

2011

The Thesis of Brian Ming Louie is approved and it is acceptable in quality and form for publication on microfilm and electronically:

_____

_____

_____

_____

Chair

University of California, San Diego

2011

TABLE OF CONTENTS

LIST OF FIGURES

LIST OF TABLES

ACKNOWLEDGEMENT

I would like to acknowledge Professor Prabhakar R. Bandaru for providing me with the research opportunity highlight in this thesis. His endless support and mentorship helped me tremendously during the course of this research project. The knowledge and incite taken away from this project and thesis is significant and could not be received from any typical graduate course.

I would also like to acknowledge Professor Renkun Chen on providing guidance and recommendations on the experimental design. His expertise in heat transfer was critical in the success of the steady state thermal conductivity apparatus.

I would also like to acknowledge Professor Sungho Jin for being a member of my committee and also lending equipment to complete tasks within this research project.

I would also like to acknowledge Thomas Chalfant for providing me with equipment and guidance needed during manufacturing of the experimental setup.

Finally, I would like to thank Rahul Kapadia without whom my research would have taken 10 times longer. His assistance and support helped me in an immeasurable way.

ABSTRACT OF THE THESIS

The Design of a Steady State Thermal Conductivity Measurement Device and Thermal Conductivity Measurement of CNT RET Polymer Composites

by

Brian Ming Louie

Master of Science in Mechanical Engineering

University of California, San Diego, 2011

Professor Prabhakar R. Bandaru, Chair

The focus of this research project was to design and build a steady state apparatus that could accurately measure the thermal conductivity of different materials. By modeling the experimental design with ASTM standards and taking care to reduce heat loss terms, a design was built that was able to accurately measure two reference materials (Pyrex and Stainless) to within 1% of their reference values. After verifying the experimental design, the thermal conductivity of the CNT RET polymer was determined and compared with 3-ω results. Both data sets from different thermal

conductivity methods yield an increase in thermal conductivity with an increase in volume percent CNT. The results from 3-ω depicted a evident percolation of thermal conductivity as a function of volume percent as compared to a linear relationship from steady state results . These differences in the thermal conductivity could have been caused by differences in testing samples, such as CNT orientation. Variations in the locations of functional groups within the CNT and location of the CNT attachment to the RET polymer chain can vary significantly from sample to sample. As a result, the varying interfaces between CNT to CNT and CNT to polymer matrix can result in significant thermal interface resistances. Future work may include research into vertically aligned CNT thermal interface materials, specifically their interface characterization. A need for accurate steady state thermal conductivity measurements and a understanding of CNT polymer composites and CNT interfaces are crucial in developing future thermal interface materials (TIMs).

INTRODUCTION:

In today's world of increasing computing demands and smaller form factor, two main factors are in the minds of many companies and researchers. How can electronics be made faster (1) and (2) even smaller than the previous generation? Moore's law states that the number of transistors in semiconductor devices will increase two fold every 18 months[2.] With this increase of power density to 100 $\left(\frac{W}{m^2}\right)$, heat transfer plays a vital part in today's microprocessors and integrated circuit chips. There are many different techniques employed to tackle IC heat generation issues such as active cooling, liquid or phase-change, or even the traditional convective cooling (i.e. heat sink). Despite the enhancement in active cooling, industry has yet to adopt such thermal management because of its complexity, cost, and reliability. As a result, the standard thermal management system that is widely adopted is still convection cooling. With limitations such as large surface area and low ambient temperature (which are critical in convective heat transfer) another solution must be developed to tackle the issue of increased heat generation. This gives rise to a new challenge of thermal management. In order to improve the efficiency of heat sinks, the thermal interface resistance/thermal boundary resistance between the IC and the heat sinks must be reduced via thermal interface materials (TIMs). TIMs are implemented to generally improve the area of contact, which is important in conductive heat transfer.

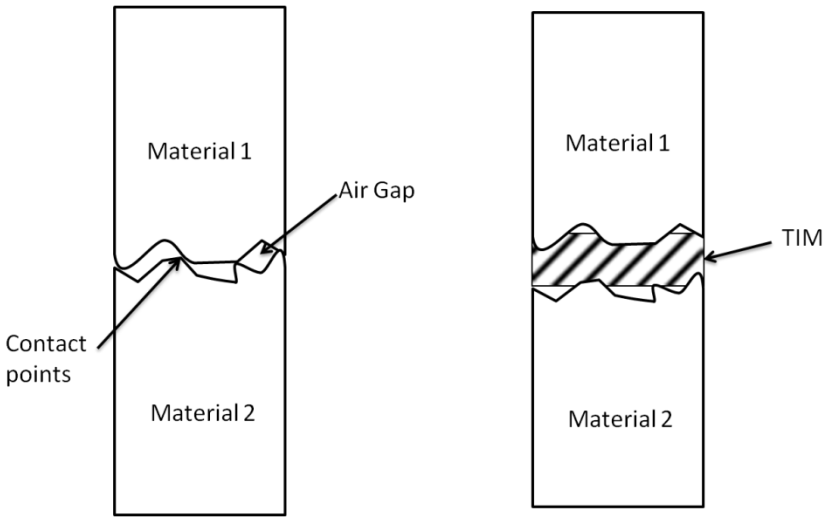

Figure 1. Schematic of Real Contact Area and Application of TIMs.

As seen in the figure above, when two surfaces are in contact, there are voids within the area of contact due to a material's surface roughness. The main modes of heat transfer at this interface involve solid to solid conduction in the area of contact and conduction/convection through fluid occupying the voids. These voids can greatly hider the effectiveness of conductive heat transfer from Material 1 to Material 2 because of the low thermal conductivity (κ) of gases, e.g. air $\left(0.024\ \frac{W}{mK}\right)$. The implementation of TIMs reduces these air gaps within the interface by filling the voids within the material's surface with high thermally conductive materials$\left(>\ 2\ \frac{W}{mK}\right)$. By developing new TIMs with high thermal conductivities $\left(>10\ \frac{W}{mK}\right)$ and low interface resistance (between TIMs and substrate) of the order of less than $\left(10^{-6}\ \frac{m^2K}{W}\right)$, the efficiency of traditional aluminum/copper based heat sinks can be greatly increased.

Over the years, various materials have been studied to tackle the thermal management issue. Some of the materials include graphite, graphene, and even carbon

nanotubes (CNT). CNTs have gained a huge research following for new TIMs because of their large aspect ratio and extremely high κ. The measured κ of MWNT at room temperature is reported to be > 3000 $\frac{W}{mK}$, which is significantly higher than even the conductivity of diamond (~2000 $\frac{W}{mK}$)[13]. As a result of this extremely high κ, CNTs are a strong contender in developing new TIMs for next-generation IC chips. CNT's extremely high κ gives rise to many different applications including CNT impregnated thermally conductive polymers which can be used for coating electronics (such as EMI shielding).

Some TIMs used today utilize low thermal conductive polymers $\left(\sim 0.2\ \frac{W}{mK}\right)$ with highly conductive filler materials $\left(> 30\ \frac{W}{mK}\right)$. Polymers make an excellent material for coatings or interface materials for their light weight nature, tunable material characteristics/properties, and manufacturability. Functional properties of the polymers that could be used to tackle this issue are elastomeric characteristics, corrosion resistance, and tunable κ.

.

RET POLYMER COMPOSITE:

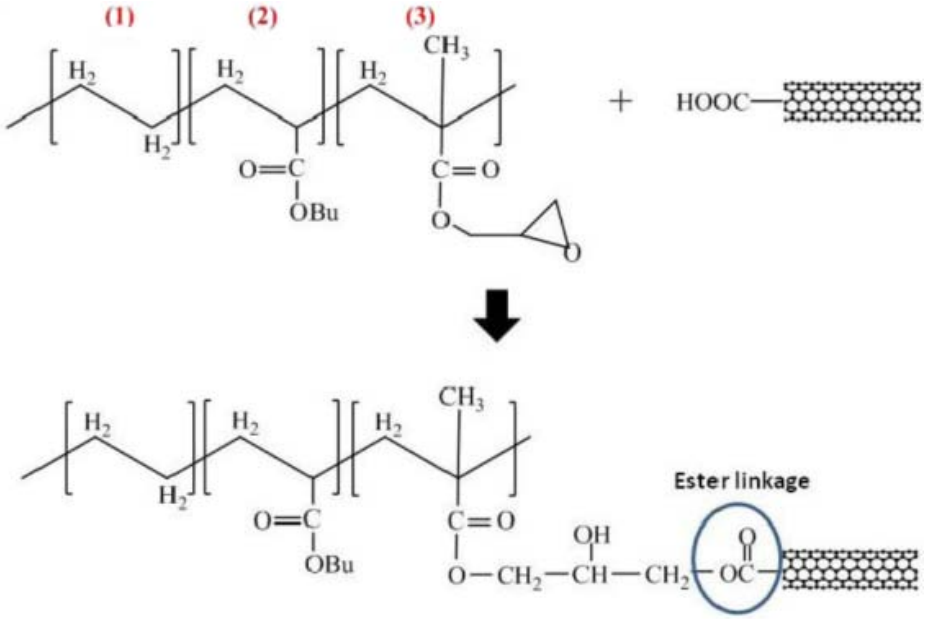

Figure 2. Schematic of Reaction Between CNT Functional Groups with Epoxy Groups on the RET. RET is Composed of (1): Polyethylene, (2) Methyl Methacrylate, and (3) Epoxide Groups.[7]

The polymer selected in this thesis is RET (reactive ethylene terpolymer - Elvaloy 4170)[7] from DuPont. This copolymer consists of three distinct monomers, ethylene backbone which provides corrosion resistance, n-butyl acrylate which provides elastomeric characteristics, and glycidyl methacrylate (GMA) which adds epoxide functionality[4]. In addition to the RET polymer, functionalized SWCNT was bonded to the RET epoxide group, as seen in Figure 2, through a chemical reaction[7]. The epoxide functionality group in this polymer plays a crucial part in the polymer's ability to be thermally conductive because it provides an anchor for the CNTs to bond to the polymer chain. A network of highly thermally conductive CNTs form a chain in which phonons may propagates effectively. The traditional method of producing a thermally conductive polymer is to mix high concentrations of metal fillers (aluminum

or copper), -around 50 volume percent, resulting in an order of magnitude increase in κ[9]. New methods utilize CNTs because of their extremely large aspect ratio (10^6) and high κ. The highly reactive epoxide group from the RET polymer provides an effective anchor of constituent ring bonds with functional groups (-OH, -COOH, etc) on the CNTs. The epoxide ring rupture can be acid catalyzed through the carboxyl groups on the functionalized CNTs. This method yields uniform CNT dispersion, seen in Figure 3[7].

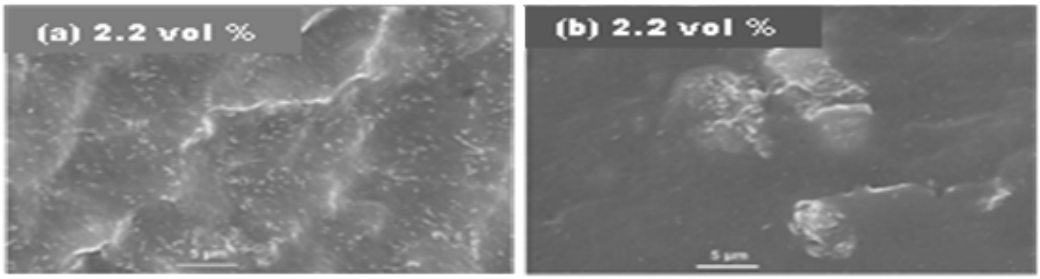

Figure 3. Scanning Electron Microscope (SEM) Micrographs illustrating Uniform Dispersion of Functionalized SWNTs in the RET Polymer at (a) 2.2 volume % CNT Filling Fractions (b) Non-Functionalized SWNTs Exhibit Clustering.[7]

To prepare the RET polymer, it was blended in toluene and heated. Separately, a mixture of sulfuric and nitric acid was used for CNT functionalization decorating the CNTs with –COOH groups. The treated CNTs were then dispersed and blended in toluene and ultrasonicated. The functionalized CNT was then added to the RET solution and re-sonicated. To remove excess solvent, the mixture was stirred and evacuated in vacuum (10^{-3} Torr) for 12 hours. Subsequently, a hot press was used to press the composites into the desired thickness, of ~ 2 mm[7].

Functionalized CNTs resolve the issues with traditional methods of mixing fillers into polymers. The latter relies on van der Waals interactions of polymer chains with CNT surfaces, while the proposed technique utilizes the much stronger chemical reaction between functional groups and reactive sites on the CNTs. The isotropic bonding of CNTs may also lead to uniform CNT dispersion, which is not evident in non-functionalized CNTs[7]. The use of CNTs may also resolves the issue with polymer embrittlement seen in high metal filler concentrations because of the low filler volume fraction (< 10%) needed with CNTs. This polymer composite has a κ percolation $\left(0.4 - 0.8\ \frac{W}{mK}\right)$ at low volume fractions (3% - 10%), which makes it an ideal replacement for high concentration metal filler polymer composites[7]. As described by Prasher, the phenomenon of percolation occurs with a formation of a continuous chain between the material via highly conductive particles, as seen in the figure below[8].

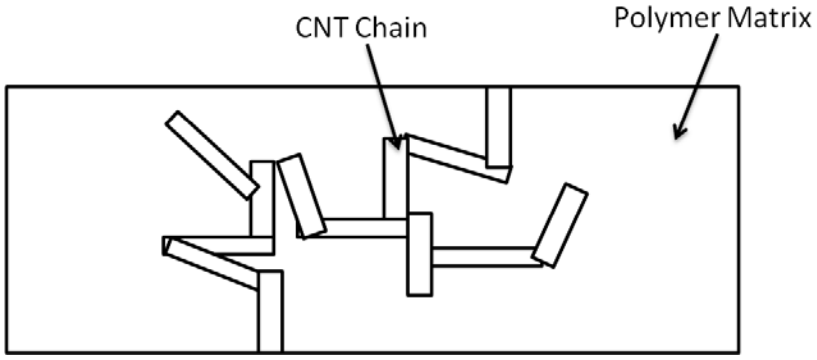

Figure 4. Diagram of a Continuous CNT Chain Within Polymer Matrix.

The percolation phenomenon in CNT RET polymer has been experimentally seen by Kim et al[7].

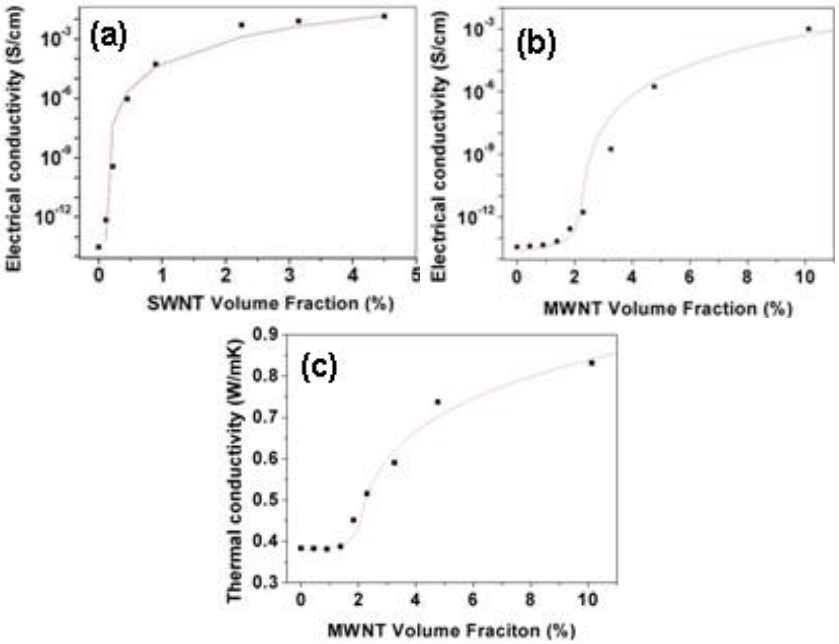

Figure 5. The Enhancement of the Electrical – (a) and (b), and Thermal Conductivity – (c) of SWNT and MWNT Based Polymers, with Increasing CNT Volume Fractions, Solid Lines Express Volume Percolation Theory.[7]

The electrical conductivity of the polymer composites and κ exhibit a percolation at low volume fractions (< 3%). It is apparent that there is a greater enhancement in the electrical conductivity (over ten orders of magnitude) compared to the approximately two-fold increase in the κ values. This percolation exhibited by the polymer composite gives rise to a plethora of applications which could include TIMs, thermally tunable materials, thermal electrics, etc...

Important aspects in characterizing thermal materials (e.g., TIMs and thermally conductive coatings) is determining proprieties such as κ and/or thermal resistance. Determining the bulk κ of a material can pose many challenges. Heat loss through convection/radiation can be extremely difficult to quantify and eliminate. There are many methods used to determine the κ of materials, such as steady state techniques

(absolute/comparative), transient techniques, the 3-ω technique, and thermal diffusivity measurments[10].

In this thesis, steady state techniques will be utilized to determine the κ of bulk materials. This technique employs and is based on the Fourier law formulation of heat conduction in materials.

BASIC THEORY:

CLASSIC FOURIER'S LAW:

Heat conduction can be defined by Fourier's Law of conduction. In a one-dimensional heat flow case, Fourier's Law states that the local heat flux in a homogenous substance is proportional to the negative temperature gradient[5]:

$$\ddot{Q} \propto -\frac{dT}{dx} \tag{1}$$

where $\ddot{Q}$ is the heat flux and $\frac{dT}{dx}$ is the temperature gradient. A constant of proportionality can be introduced to yield the most common formulation of Fourier's Law of Conduction[5]:

$$\dot{Q}_{cond} = -\kappa A \frac{dT}{dx} \tag{2}$$

where κ is known as the thermal conductivity and *A* is the effective area. To further understand where this κ term is derived from, one could examine the kinetic theory of gas. Although this theory was derived for gas particles, one could treat heat transfer in a solid as heat transferred through lattice vibrations/phonons.

KINETIC THEORY:

The kinetic theory for the κ of gases can be defined as (in the x-direction)[10]:

Figure 6. Diagram of Thermal Conductivity for Kinetic Theory.

$$E_{TOTAL} = c\frac{\partial T}{\partial x}l_x \tag{3}$$

where E_{TOTAL} is the total energy, c is the heat capacity, $\frac{\partial T}{\partial x}$ is a temperature gradient, and l_x is the mean free path. Eq. (3) can be further modified by substituting the particle velocity v_x and relaxation time τ into the mean free path resulting in:

$$E_{TOTAL} = c\frac{\partial T}{\partial x}v_x\tau \tag{4}$$

Equation (4) can then be examined in terms of the net energy flux:

$$Net\ Energy\ Flux = (nv_x)c\frac{\partial T}{\partial x}v_x\tau \tag{5}$$

where nv_x is the net particle flux. This equation can be further reduced to:

$$Net\ Energy\ Flux = C\frac{\partial T}{\partial x}{v_x}^2\tau \tag{6}$$

where *C* is the total heat capacity ($C = nc$). To generalize the equation to apply to 3 dimensional cases, the velocity term can be portrayed through an average velocity given by:

$${v_x}^2 = {v_y}^2 = {v_z}^2 = \frac{1}{3}v^2 \tag{7}$$

By substituting Eq. (7) back into Eq. (6), the equation now reduces into the form:

$$Net\ Energy\ Flux = \frac{1}{3}Cv^2\tau\nabla T \tag{8}$$

Relating Equation (8) with the standard Fourier Law, Eq. (8) can then be generalized for κ to the following form[10]:

$$\kappa = \frac{1}{3}Cvl \tag{9}$$

where κ is the thermal conductivity, C is the total specific heat, v is the average particle velocity, and l is the mean free path.

EXPERIMENTAL DESIGN:

Thermal conductivity of materials has been an area of research for many decades. There are a plethora of thermal conductivity measurement techniques spanning from steady state methods and transient methods. In this thesis, steady state methods utilizing Fourier's Law of Conduction were analyzed. Steady state thermal conductivity test methods from the American Society of Testing and Materials (ASTM) were studied and used as a baseline to develop the test apparatus used in this Thesis. ASTM has published two different test methods (D 5470/ E 1225) for measurement of κ via steady state methods. A brief summary of these two test methods are listed below.

ASTM STANDARDS:

ASTM E 1225 is a test method for determination of κ via the steady state technique. This test method is intended for materials with an effective thermal conductivity range $0.2 < \kappa < 200 \left(\frac{W}{mK}\right)$ over a temperature range between 90 and 1300 (K). A schematic of the test apparatus is portrayed below.

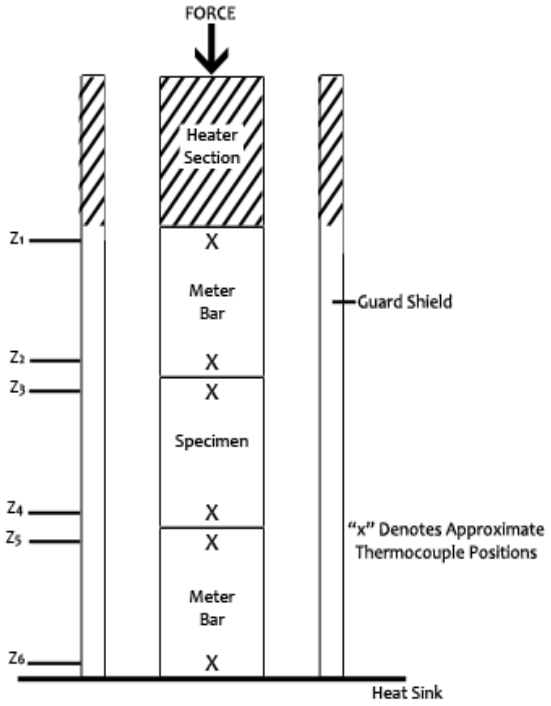

Figure 7. Schematic of Test Apparatus for ASTM E 1225.

Meter bars are defined as a piece of reference material (of known κ) used to measure heat flux via an imposed temperature gradient. When selecting meter bar materials, this standard suggests that the thermal conductance of the meter bars $\frac{\kappa_M}{l_M}$ be similar to the thermal conductance of the sample $\frac{\kappa_S}{l_s}$. This $\frac{\kappa}{l}$ ratio is important because uniform heat flux throughout the apparatus is assumed. As a result, Eq. (2) can be re-written as:

$$\kappa_m \left(\frac{dT}{dx}\right)_m = \kappa_s \left(\frac{dT}{dx}\right)_s \tag{10}$$

where κ_i is the corresponding thermal conductivity (meter bar/sample) and $\left(\frac{dT}{dx}\right)_i$ is the corresponding temperature gradient. By having a similar thermal conductance of both meter bars and sample, one can expect a similar temperature drop through the meter bars and sample.

To determine the κ, a series of calculations must be made. The measured temperatures at each meter bar are recorded and the heat flux per meter bar is determined via:

$$q'_T = \kappa_M \frac{T_2 - T_1}{Z_2 - Z_1} \tag{11}$$

$$q'_B = \kappa_M \frac{T_6 - T_5}{Z_6 - Z_5} \tag{12}$$

where T_i corresponds to the temperature at Z_i and κ_M is the κ of the meter bar. This standard states that the values for q'_T and q'_B should be within ± 10% of each other. The sample κ is then calculated via:

$$\kappa_S = \frac{(q'_T + q'_B)(Z_4 - Z_3)}{2(T_4 - T_3)} \tag{13}$$

ASTM D 5470 is a test method for measurements of thermal impedance and calculation of the κ of thermally conductive electrical insulation materials. A schematic of the test apparatus is portrayed below.

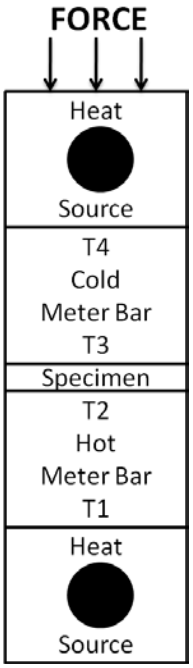

Figure 8. Schematic of Test Apparatus for ASTM D 5470.

This method is also considered a steady state technique, which means temperature at a given distance remains constant. In this method, equilibrium is attained when at constant power, 2 sets of temperature reading measured at 5 minutes intervals differ by less than ± 0.1 °C.

Through the measured equilibrium temperatures, the heat flow in the meter bars can be calculated through the following equations:

$$Q_{12} = \frac{\kappa A}{d}(T_1 - T_2) \quad (14)$$

$$Q_{34} = \frac{\kappa A}{d}(T_3 - T_4) \quad (15)$$

$$Q = \frac{Q_{12}+Q_{34}}{2} \quad (16)$$

where:

Q_{12} is the heat flow in the hot meter bar

Q_{34} is the heat flow in the hot meter bar

Q is the average heat flow in the specimen

A is the cross-sectional area

$T_1 - T_2$ is the temperature difference between temperature sensors of the hot meter bar

$T_3 - T_4$ is the temperature difference between temperature sensors of the hot meter bar

d is the distance between temperature sensors in the meter bar

The temperature of the sample surface touching the hot meter bar is:

$$T_H = T_2 - \frac{d_B}{d_A}(T_1 - T_2) \quad (17)$$

T_H is the surface temperature of the sample measured from the hot meter bar

T_1 is the higher temperature of the hot meter bar

T_2 is the lower temperature of the hot meter bar

d_A is the distance between T_1 and T_2

d_B is the distance between T_2 and the top surface of sample in contact with the hot meter bar

$$T_C = T_2 - \frac{d_D}{d_C}(T_3 - T_4) \quad (18)$$

T_C is the surface temperature of the sample measured from the cold meter bar

T_3 is the higher temperature of the cold meter bar

T_4 is the lower temperature of the cold meter bar

d_C is the distance between T_3 and T_4

d_D is the distance between T_3 and the bottom surface of sample in contact with the cold meter bar

To calculate the thermal impedance $\left(\frac{Km^2}{W}\right)$, the following equation is used:

$$\theta = \frac{A}{Q}(T_H - T_C) \quad (19)$$

By plotting thermal impedance versus sample thickness, interface resistance can be obtained though the y-intercept of this plot. The slope of this curve is the reciprocal of the sample κ.

To test the precision of these ASTM test methods, a round robin methodology was implemented with five different materials and six different laboratories. From the data obtained from the round robin, it was concluded that the κ values for the same sample material measured by the different laboratories fell within 18% of each other. This figure indicates the general accuracy of thermal conductivity measurements.

INITIAL TEST APPARATUS:

The initial experimental design was modeled after both ASTM standards (E 1225 and D 5470) highlighted above. Both test methods, utilize Fourier's Law of Conduction, Eq. (2). Both methods assume uniform 1-D heat flux down the meter bars and sample. Since the meter bars are made of a known material, the heat flux ($\frac{\dot{Q}}{A}$) traveling through the meter bars and sample can be estimated using Eq. (2) and from the known κ of the meter bars, and temperature gradients obtained from the meter bars. Similar to ASTM D 5470, the surface temperatures are not directly measured but calculated instead using the determined heat flux of the meter bar, as seen Eq. (17) and Eq. (18). To determine the κ of the sample, Eq. (2) can be re-arranged to:

$$\kappa = -\frac{Q}{A}\frac{dx}{dT} \tag{20}$$

A schematic of this experimental design is portrayed below.

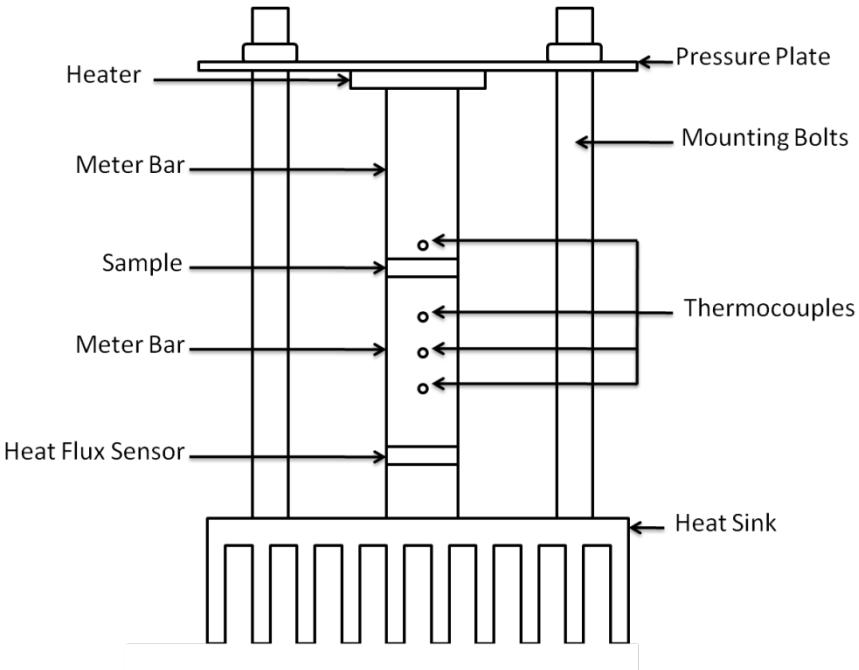

Figure 9. Initial Proposed Design for Steady State Thermal Conductivity Measurement Device.

The first experimental design utilized an Omega SRF Silicon Heater as the heat source to provide uniform heat flow to the meter bars and sample. The meter bars were machined out of Stainless Steel (303) to a length of four centimeters each. A series of three Omega Ready-Made K-type thermocouples (TC) were embedded in the lower meter bar one centimeter apart and one TC was embedded in upper meter bar near the surface of the sample. Holes roughly of the same diameter of the TCs (0.81 mm) were drilled in each meter bar. This allowed the TCs to be press fit into each meter bar, which decreased their thermal contact resistance by essentially reducing gaps between the two surfaces (TC junction and meter bar). To help further reduce this contact resistance and improve the accuracy of the TC measurements, each TC was covered in ArticSilver, ~ $\kappa = 8\ \left(\frac{W}{mK}\right)$[13].

Table 1. Thermal Conductivity of Thermocouple Materials.[5]

Wire Material	k (W/mK)
Copper	385
Constantan	23
Iron	73
Chromel	17
Alumel	48

Utilizing a TC type (T,J, or K) with materials that have the lowest κ is important because it reduces conduction heat loss through the TC wires. Heat loss through the TC can be estimated by using Eq. (2). The thermal conductance (C_T), the quantity of heat that passes in a unit of time through a given area, of the TC wire can also be determined via[5]:

$$C_T = \frac{\kappa A}{L} \tag{21}$$

Table 2. Estimated Thermal Conductance and Heat Loss for Various Thermocouple Types.

Thermocouple Type	Thermal Conductance (W/K)	Heat Loss Per Thermocouple(mW)
K	2.20E-04	5.49
J	3.25E-04	8.11
T	1.38E-03	34.49

The table above was calculated assuming a TC length of 0.152 (m) and a diameter of 0.81 (mm), equivalent of 20-AWG wire. K-type TC were utilized in this design because of their lowest thermal conductance, estimated to be 0.00022 $\left(\frac{W}{K}\right)$, which correlates to the lowest heat loss per TC estimated at 5.49 (mW). Keithley 2700 and LabView were used to obtain the temperature profile of the meter bars. The temperature profiles were allowed to reach steady-state as defined by ASTM D 5470.

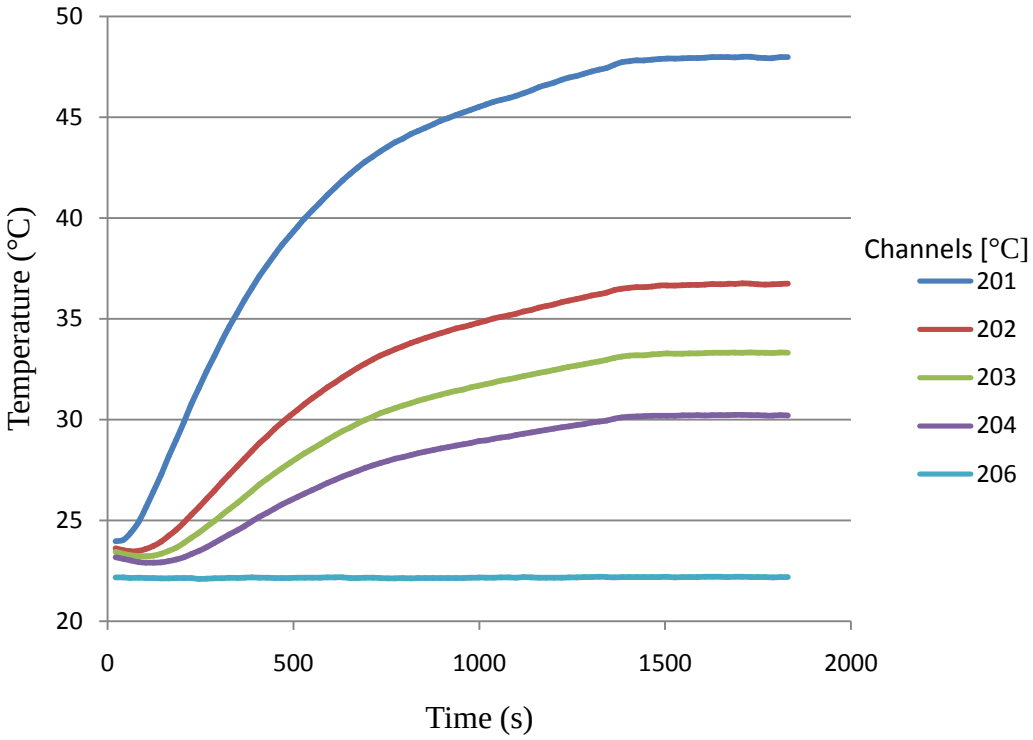

Figure 10. Measured Thermocouple Temperature via LabView.

After measuring the temperature at each meter bar, the heat flux experienced at the lower meter bar is calculated by plotting the measured temperature versus TC position.

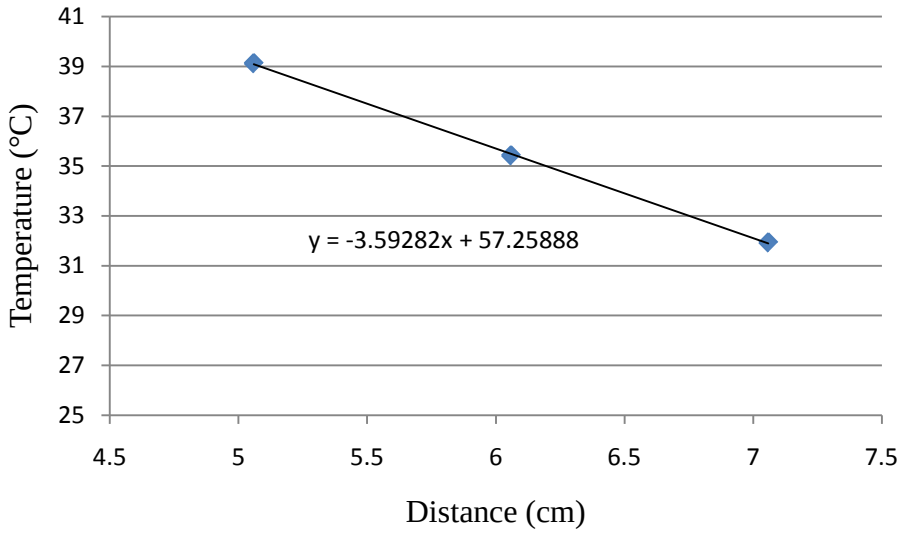

Figure 11. Measured Temperature vs. Position.

The slope of the measured temperature versus position plot, seen in the figure above, is the heat flux experienced by the meter bar. To further validate the calculated heat flux value determined through the meter bar, a Vatell heat flux sensor (BF-02) was mounted underneath the lower meter bar. The heat flux sensor provided a voltage reading for a specified heat flux.

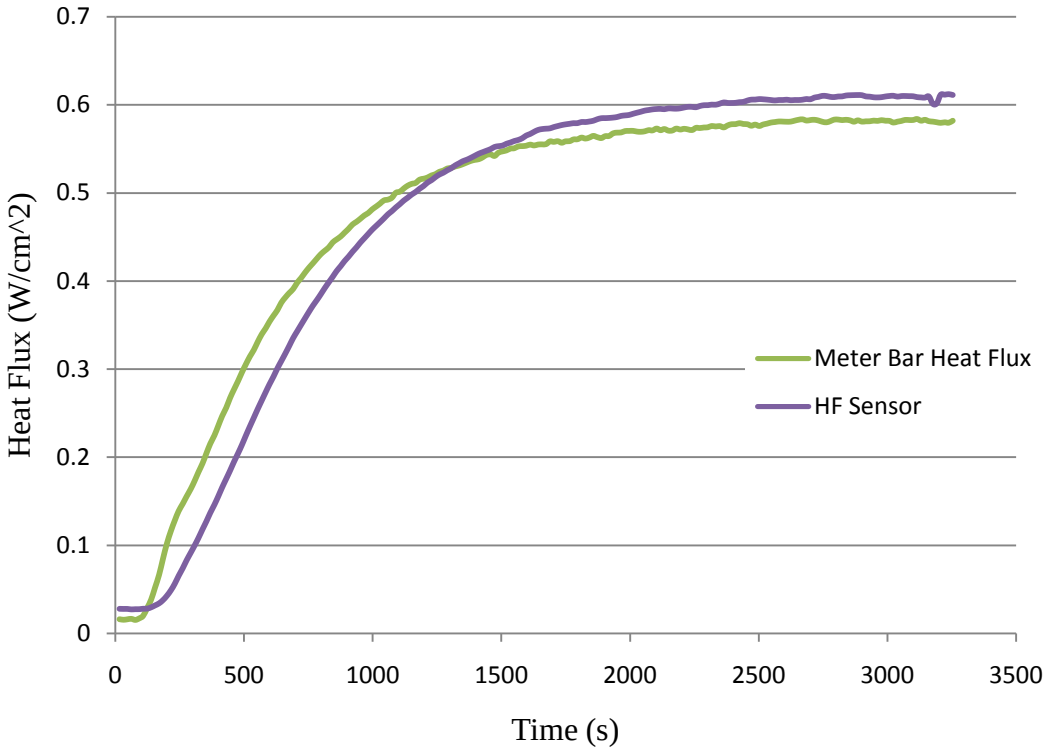

Figure 12. Measured Heat Flux via Heat Flux Sensor and Meter Bar.

As anticipated the measured heat flux from BF-02 is in good agreement with the measured heat flux from the meter bar, as seen in the figure above. From the determined heat flux from both meter bar and heat flux sensor, the κ of the sample (Pyrex) can be determined via Eq. (20).

Table 3. Thermal Conductivity of Pyrex Sample.

	k of Sample (W/mK)	Percent Error (%)
From Meter Bar	1.49	29
From Heat Flux Sensor	1.56	36

The κ of the Pyrex sample determined from the meter bar was 1.49 $\left(\frac{W}{mK}\right)$ and 1.56 $\left(\frac{W}{mK}\right)$ from the heat flux sensor. Based on these results, a 29 and 36 percent error is obtained when comparing with a κ of 1.15, given by literature and supplier[5,10]. To

improve the accuracy and functionality of the initial experimental design, many design changes can be implemented to the test apparatus. One major flaw in the initial design was the mounting of the heat flux sensor, as seen in the figure below.

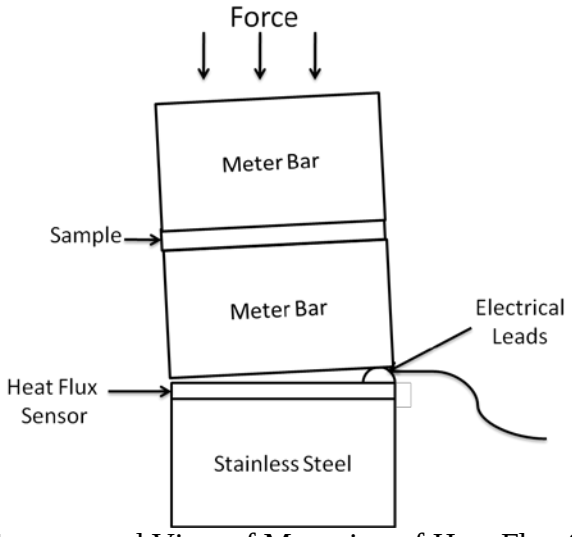

Figure 13. An Exaggerated View of Mounting of Heat Flux Sensor in Initial Experimental Design (Not to Scale).

Since the leads of the sensor yield a non-uniform surface, equal pressure distribution on the sample was extremely hard to achieve. Heat loss through convection/radiation, and parasitic heat conduction, was also another area of concern. We first consider the parasitic contributions.

Conduction heat loss can be evident in the form of conduction through the TCs. To reduce this effect, it is recommended that TCs utilized in the experimental apparatus are as small as possible without sacrificing accuracy. Conduction via TCs could be estimated by Eq. (2).

Table 4. Heat Loss through Various Thermocouple Sizes.

Thermocouple Gauge (AWG)	Diameter (m)	Thermal Conductance (W/K)	Heat Loss Per Thermocouple (mW)
20	8.10E-04	2.20E-04	5.49
22	6.50E-04	1.42E-04	3.54

As seen in the table above, by reducing the diameter of the K-type TCs from 0.81 (mm) to 0.65 (mm), the heat loss per TC is reduced 36% from 5.49 (mW) to 3.54 (mW). The heat loss due to conduction through the 22 gauge TC wire is significantly smaller than the operating conditions of the experimental apparatus (~ 0.6 W).

Heat convection is another issue that can greatly affect the steady state thermal conductivity measurements, especially when the apparatus is open to the ambient environment (laboratory). A possible method to reduce this effect, is to perform the experiment in vacuum. Convective heat transfer can be described by Newton's Law of Cooling:

$$\dot{Q}_{conv} = h_{conv} A(T_s - T_\infty) \tag{22}$$

where h_{conv} is the heat transfer coefficient, A is the surface area, T_s is the surface temperature, and T_∞ is the ambient temperature. Typical values for h_{conv} for air range from 5-25 $\left(\frac{W}{m^2 K}\right)$. Finally, radiation heat losses can also have an effect on the thermal conductivity measurement. Radiation loss can be expressed as[6]:

$$\dot{Q}_{rad} = \varepsilon A \sigma \left({T_1}^4 - {T_2}^4\right) \tag{23}$$

where ε is the emissivity, A is the effective area, σ is the Stefan-Boltzmann constant, and T_1 and T_2 are surface temperatures. Heat loss due to radiation can be minimized by reducing the "hot" temperature, reducing the effective area, and/or reducing emissivity.

FINAL EXPERIMENTAL DESIGN:

After closely analyzing the highlighted flaws with the initial experimental design, a new design was developed to tackle the highlighted issues.

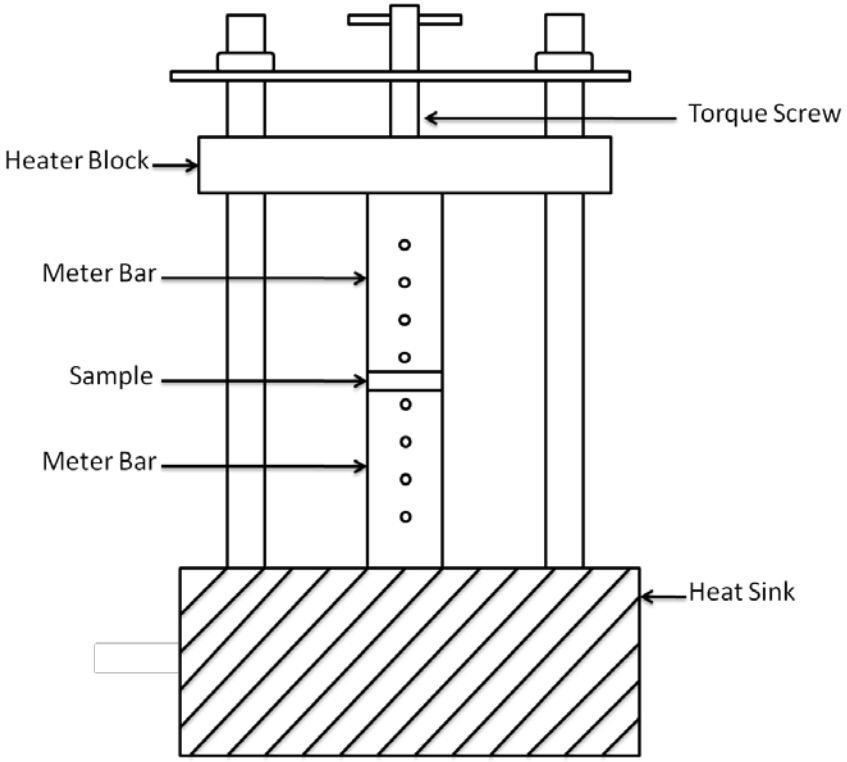

Figure 14. Final Design of Steady State Thermal Conductivity Measurement Device.

The final experimental design, seen in the Figure 14, consists of a cartridge heater mounted in a stainless steel block which provides uniform heat to the meter bars. A threaded rod connected to the heater block was used to apply constant and uniform pressure to the meter bars and sample. Two 303 stainless steel meter bars four centimeters long were utilized to transfer heat in and out of the sample. This length and material choice for the meter bars was chosen because of their $\frac{\kappa_M}{l_M}$ ratio. Assuming a sample κ of 0.8 $\left(\frac{W}{mK}\right)$ and a length of 2 mm, a $\frac{\kappa_S}{l_S}$ ratio of 400 is obtained. To yield

the same $\frac{\kappa_M}{l_M}$ ratio, a length of 4 cm must be used, if assuming a $= 16\ \left(\frac{W}{mK}\right)$. Stainless steel is a perfect material for the meter bars because it fits within this criterion $\left(\kappa_{ss} \approx 16\ \frac{W}{mK}\right)$ and was easily machinable.

As mentioned in the initial design, K-type TCs were the ideal TC type because of their low thermal conductance, which reduces conduction heat loss through the TC. Three K-type TCs were mounted equal distances from each other (~ 1 cm) and a fourth K-type TC mounted near the surface (< 2 mm) in each meter bar. This fourth TC was specifically utilized to accurately extract the surface temperatures of the sample. Since embedding TCs into the sample was not feasible, the surface temperatures at the sample were extrapolated via the following equation:

$$T_s = \frac{dT}{dx}x + C \tag{24}$$

where $\frac{dT}{dx}$ is the temperature gradient, x is the position, and C is the y-intercept obtained from a temperature versus position plot. Twenty two gauge K-type TCs, instead of 20 AWG TCs, were implemented to further reduce conduction heat loss, mentioned earlier. By removing the heat flux sensor from the experimental design, the issue of non-uniform pressure distribution is avoided. Since the heat flux sensor served as a validation measurement for the heat flux derived from the lower meter bar, an additional series of TCs were mounted in the upper meter bar to examine the heat flux in the upper meter bar. The temperature profile of the entire meter bars and sample surface temperature were determined via these embedded TCs. An interesting result that was not apparent in the initial design became evident. The heat flux between the

upper and lower meter bars were in fact considerably different, as seen in the table below.

Table 5. Calculated Heat Flux from Upper and Lower Meter Bars.

	Heat Flux $\left(\frac{W}{m^2}\right)$
Upper Meter Bar	4068
Lower Meter Bar	2935
Percent Difference between Upper and Lower Bars(%)	39%

This experimental result is of huge concern because of the assumption that this experimental design and ASTM standards are based on is uniform heat flow throughout the meter bars and sample. The difference in heat flux could have been a result of heat loss through various heat loss mechanism incorporating conduction, convection, and/or radiation.

To reduce convective effects the experiment was performed under vacuum. As seen in Eq. (22) a governing term in convective heat transfer is h_{conv}. The convective heat transfer coefficient can be related to pressure using the following relationships:

$$Nu = 0.478 G_r^{\frac{1}{4}} \tag{25}$$

where Nu is the Nusselt number that describes a ratio of convective to conduction heat transfer across a boundary and G_r is Grashof number the ratio of the buoyancy to viscous force acting on a fluid. The Grashof number is proportional to pressure via:

$$G_r \propto P^2 \tag{26}$$

where P is the pressure. Pressure relates to the Nusselt number via:

$$Nu \propto P^{\frac{1}{2}} \tag{27}$$

Relating Eq. (24,25, and 26) together yields:

$$h_{conv} \propto P^{\frac{1}{2}} \tag{28}$$

Normal atmospheric pressure is $P_1 = 1.0132\ x\ 10^5\ \left(\frac{N}{m^2}\right)$ and the pressure under vacuum is $P_2 = 1.332\ \left(\frac{N}{m^2}\right)$ which is equivalent to 10 millitorr. Using Eq. (27) an estimate of the heat transfer coefficient at 10 millitorr can be calculated via:

$$h_2 = 3.6\ x\ 10^{-3} h_1 \tag{29}$$

Assuming $h_1 \approx 5\ \frac{W}{mK}$ (air at standard temperature and pressure)[5], $h_2 = 0.018\ \frac{W}{mK}$. Based on this estimation, convective heat transfer can be neglected when the experiment is performed under vacuum (~ 10 millitorr).

Since the design utilized a vacuum chamber, the standard technique of heat sinking to the base temperature via forced convection (heat sink and fan) would no longer work. A possible solution would be to actively cool the lower meter bar via water cooling. Water cooling requires a closed loop, consisting of a pump, heat exchanger, cooling block, and a liquid feed through for the vacuum chamber. To add the water cooling system to the experimental setup was far too complex and was not feasible. To resolve this issue and provide ample sinking to the lower meter bar, a large aluminum stock (diameter = 6 in, height = 12 in) was mounted to the bottom of the vacuum chamber. The large aluminum stock and vacuum chamber acted like a large passive heat sink.

Lastly, radiation effects must be minimized. As stated earlier, reduction in the effective area, "hot" temperature, and emissivity is needed to reduce radiative heat

transfer. Reducing emissivity is one of the most common practices to reduce radiation heat loss. This is commonly done through the implementation of heat shields.

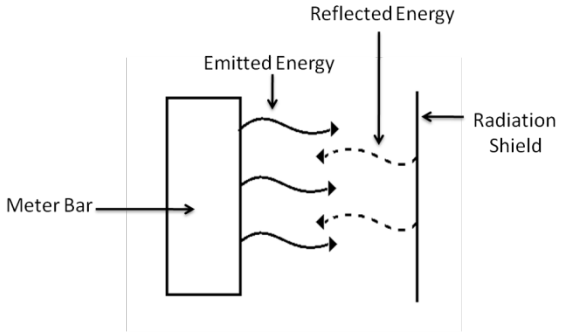

Figure 15. Schematic of Effect of Radiation Shield on Thermal Radiation.

The meter bar which is made out of stainless steel has an $\varepsilon \approx 0.35$. Emissivity can range from 1 (perfect black body) to 0 (perfectly reflective material). The implementation of a radiation shield is to reflect some of the emitted radiation from the meter bar back to itself, as seen in the figure above. The radiation shields are made of highly reflective materials, such as aluminum foil, polished metals, etc.., usually ranging in $\varepsilon < 0.1$. The final design implemented a radiation shield made from PVC coated Mylar which enclosed the meter bars and sample. The Mylar coating used is a SOL Thermal Blanket purchased from REI which has an $\varepsilon \approx 0.03$.

Table 6. Radiation Effect on Heat Flux Measured by Reference Meter Bars.

	Q" - Top $\left(\frac{W}{m^2}\right)$	Q" - Bottom $\left(\frac{W}{m^2}\right)$	QTop - QBottom Difference (%)
No Radiation Shield	4068	2935	39
Radiation Shield	3700	3187	16

As seen in Table 6, the addition of a heat shield significantly reduced the heat flux difference between the top meter bar and the bottom meter bar. With no radiation shield, the heat flux difference between the two reference meter bars was ~ 38% and

the addition of a radiation shield reduced the difference to ~ 16%. Since the experiment was performed under vacuum, convection effects can be neglected. As a result, the bulk of heat loss, which is depicted in the different heat fluxes measured by the meter bars, was caused by either conduction through the TCs or heat loss due to radiation.

RESULTS/DISCUSSION:

To verify/calibrate the steady state thermal conductivity apparatus design, the κ of Pyrex (which is a common standard for thermal measurements) and 303-stainless steel samples were determined. Listed below is a table of the determined thermal conductivities.

Table 7. Measured Thermal Conductivity of Two Reference Materials (Pyrex and Stainless Steel)

Material	Steady State - Thermal Conductivity $\left(\frac{W}{mK}\right)$	Theoretical Thermal Conductivity $\left(\frac{W}{mK}\right)$	Percent Error (%)
303-Stainless Steel	16.2 ± 1.2	16.3	0.5
Pyrex	1.1 ± 0.1	1.15	0.6

As seen above, the calculated steady state κ and theoretical κ are in good agreement for both materials. The measured values are within one percent of their κ values given by literature[5,10]. Since both κ ranges are in good agreement, it was concluded that the design was adequate for accurately measuring the κ of the CNT RET polymer.

Unlike the two test materials mentioned earlier, the CNT RET polymer is an elastomer with porosity. As a result, it is important to characterize the contact resistance/thermal boundary resistance (TBR) between the stainless steel reference blocks, interface material, and CNT RET polymer. The interface between the stainless steel reference blocks and sample could be modeled as a series of thermal resistors, as seen below.

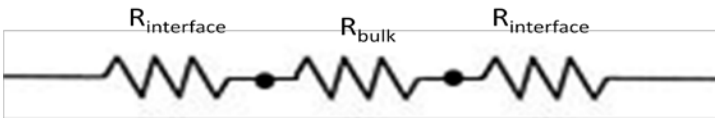

Figure 16. Schematic of Total Thermal Resistance Between Sample and Interface.

$R_{interface}$ represents the interface resistance consisting of the reference stainless steel block to the TIM to the sample and R_{bulk} represents the bulk thermal resistance of the sample. The net thermal resistance for the bulk and interface material can be written as:

$$R_{total} = R_{bulk} + R_{interface} \tag{30}$$

where $\left(R = \frac{L}{\kappa A}\right)$. Substituting for R_{bulk} yields

$$R_{total} = \frac{L}{\kappa A} + R_{interface} \tag{31}$$

where L is the characteristic length of the specimen and A is the characteristic area. Taking Eq. (31) and normalizing with respect to area and differentiating with respect to (L) yields

$$\frac{dR_{total}\,A}{dL} = \frac{1}{\kappa} \tag{32}$$

By plotting the thermal impedance, defined as $\left(\frac{L}{\kappa}\right)$, versus sample thickness (L), the interface resistance, $R_{interface}$, can be extracted (y-intercept). The slope of this plot is the inverse of the bulk κ.

To obtain the thermal resistance of the CNT RET polymer, various RET polymer samples at varying thickness were tested. A plot of the RET thermal impedance versus sample thickness was produced and depicted below.

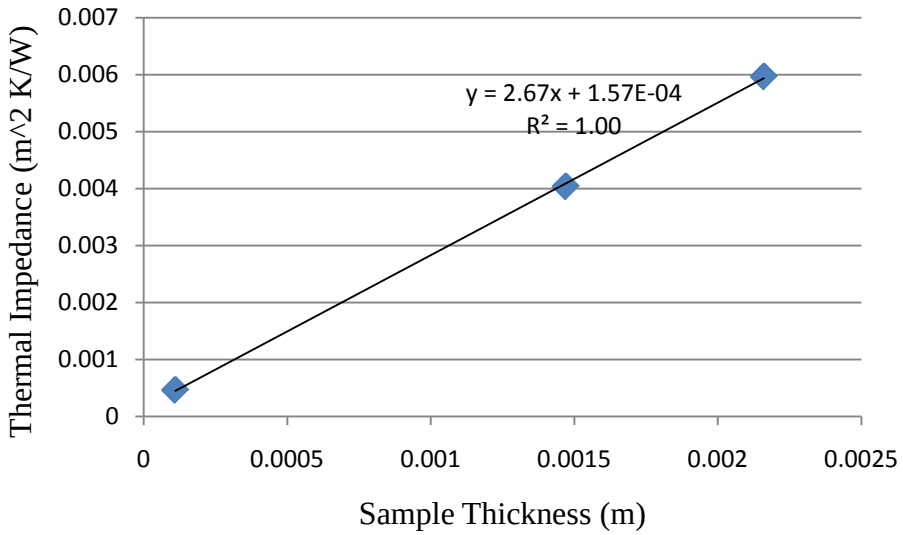

Figure 17. RET Thermal Resistance vs. Sample Thickness

Based on the graph above, the calculated thermal interface resistance for RET polymer is 0.00016 $\left(\frac{m^2K}{W}\right)$ and the κ of RET polymer is 0.37 $\left(\frac{W}{mK}\right)$, which is in good agreement with data collected via 3-ω method from B/Kim $\left(0.38\ \frac{W}{mK}\right)$. Assuming the determined thermal interface resistance for the stainless steel block to ArticSilver to RET polymer is similar $\left(R_{interface}\ \approx 0.0001\ \left(\frac{m^2K}{W}\right)\right)$ to that of the stainless steel block to ArticSilver to CNT RET polymer, the bulk κ of the CNT RET polymer can be determined through Eq. (29). This is a valid assumption because one can assume similar interface interactions between the RET polymer and the CNT RET polymer composite.

The κ of CNT RET polymer at various CNT volume percentages were measured via the steady state method described.

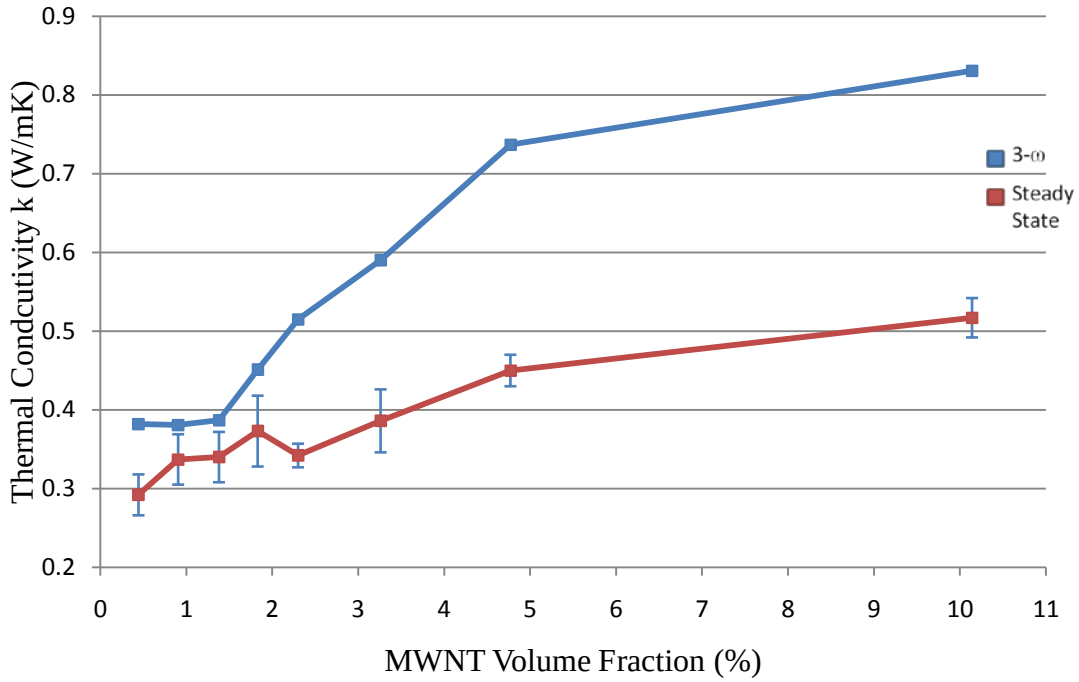

Figure 18. Thermal Conductivity of CNT RET Polymer via 3-Omega and Steady State Method.

As seen in the figure above, the red data series is the measured κ of the CNT RET polymer at various CNT volume percentages using steady state method. The blue data series is the measured κ of the CNT RET polymer via 3-ω method. The results from the 3-ω method depict a evident percolation in κ which can be described by:

$$\kappa \sim \begin{cases} (\phi_c - \phi)^{-p}, \phi_c < \phi \\ (\phi - \phi_c)^{q}, \ \phi > \phi_c \end{cases} \tag{33}$$

where ϕ is the volume fraction, ϕ_c is the threshold volume fraction for the onset of thermal percolation and p and q are the critical exponents in the respective regimes. The result from the steady state method, highlighted in red, does not closely follow this percolation trend. The data set has a more linear relationship of κ with volume fraction. The 3-ω results also show a higher increase in κ from ~ 0.4 $\left(\frac{W}{mK}\right)$ to ~ 0.8

$\left(\frac{W}{mK}\right)$ as compared to ~ 0.3 $\left(\frac{W}{mK}\right)$ to ~ 0.5 $\left(\frac{W}{mK}\right)$ from the steady state method. This noticeable discrepancy between the two measurement techniques could have manifested due to several aspects, which will be discussed later.

An important characteristic of TIMs is the variation of their thermal properties as a function of applied pressure. This characteristic is important because it highlights the thermal properties in a real world application, where TIMs would be pressed in between an IC chip and a heat sink.

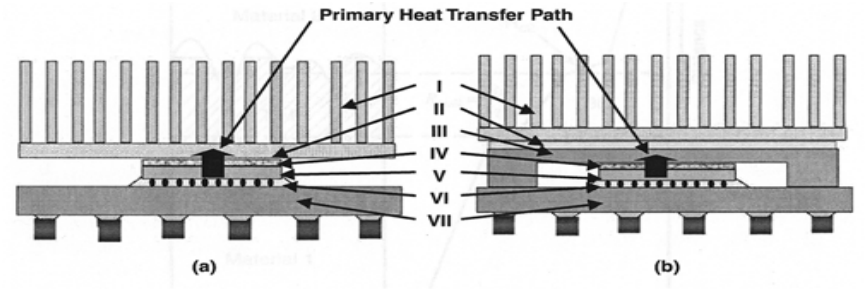

Figure 19. Schematic Illustration of the Two Thermal Architectures (a) Architecture I Typically Used in Laptop Applications and (b) Architecture II Typically Used in Desktop and Server Applications. I - Heat Sinks, II - TIM, III - IHS, IV - TIM, V - Die, VI - Underfill, and VII - Package Substrate.[8]

Applied pressure can reduce the thermal contact resistance because of the reduction in air gaps within the interface and an increase in the contact area involving solid-to-solid conduction. Prasher discussed an empirical relationship between solid-solid contact resistance (R_{CS}) as:

$$R_{CS} = \frac{0.8\sigma}{m\kappa_h}\left(\frac{H}{P}\right)^{0.95} \tag{34}$$

where $\sigma = (\sigma_1^2 + \sigma_2^2)^{0.5}$, σ is the root mean square roughness, m is the mean asperity slope, H is the micro-hardness, which is known as the hardness testing of a material with low applied loads, of the softer material, and P is the applied pressure, and

$\kappa_h = \frac{2\kappa_1\kappa_2}{\kappa_1+\kappa_2}$ is the harmonic mean κ of the materials constituting the interface. Prasher also depicts the variation of R_{CS} between copper and silicon for a pressure range (5-150 psi).

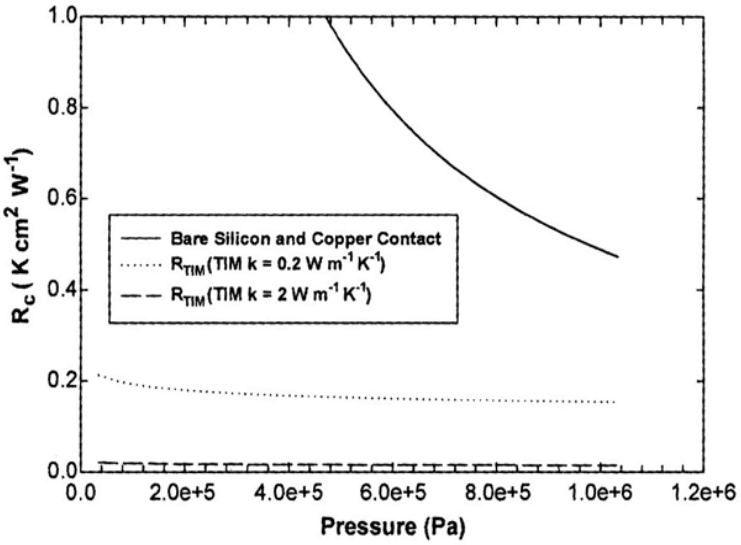

Figure 20. Thermal Resistance without TIM and in Presence of Ideal TIM.

As seen in the figure, the bare silicon and copper R_{CS} is very high at low pressures and decreases with increased pressure. This high contact resistance can arise from the air gaps between two solid surfaces, evident at low pressures, and the natural roughness of the two materials in contact.

The effects of pressure on the total thermal resistance was analyzed for a 20% CNT polymer sample. As pressure dependence can play a vital role into characterizing TIMs, this allows one to look at the possibility of producing a thermally “tunable” material.

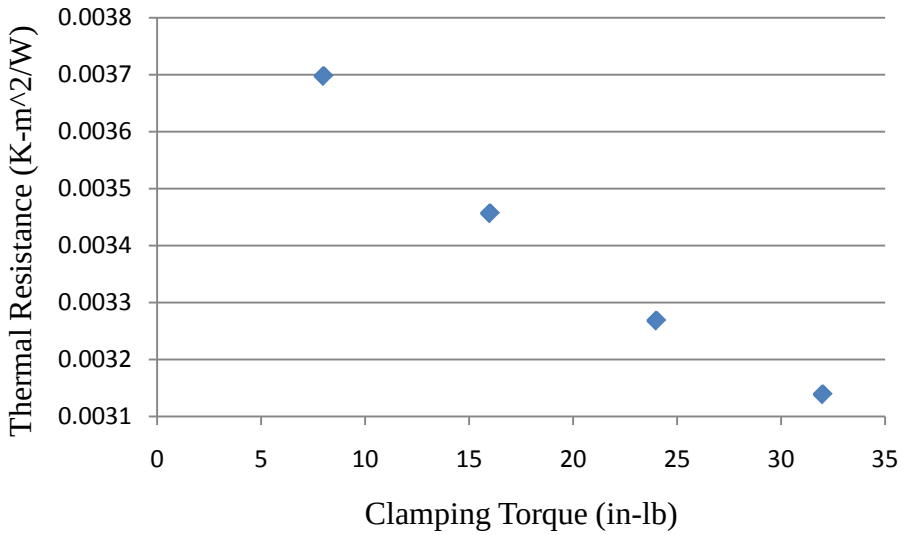

Figure 21. Thermal Conductivity of 20% CNT Polymer at Various Clamping Torque, $(\mathbf{1}\ \boldsymbol{in-lb} = \mathbf{0.13}\ \boldsymbol{Nm})$.

The figure above depicts the total thermal resistance as a function of clamping torque. This plot portrays a similar trend as seen in Figure (20). From Eq. (30), the total resistance can defined as the bulk thermal resistance plus the interface resistance. Assuming the bulk/intrinsic thermal resistance of the CNT polymer composite remains constant at varying pressures, the decrease in thermal resistance seen in Figure (20) could be caused by a decrease in contact resistance. An increase in pressure results in a reduction of air gaps within the interface and a better solid-solid contact between the polymer composite and the meter bars.

The variation in κ measurements from the two methods (steady state and 3-ω) could be caused by many factors. One possible explanation for the differences in κ values could simply be due to a variation in sample arrangement and/or composition. Since the epoxide group forms on the CNT in a random fashion, the attachment to the polymer (RET) chain is unpredictable. The main modes of heat transfer occur through

the CNTs. The linkage of CNTs can be random and are not necessarily aligned along the tube axis, as seen below.

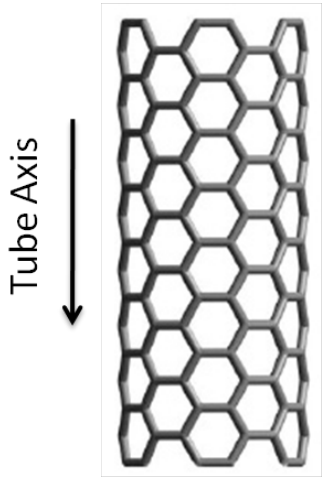

Figure 22. Schematic of CNT .

Some CNTs can be linked together perpendicular to the tube axis and some can be mix-matched and vice-versa. A possible depiction of the CNT linkage can be found below.

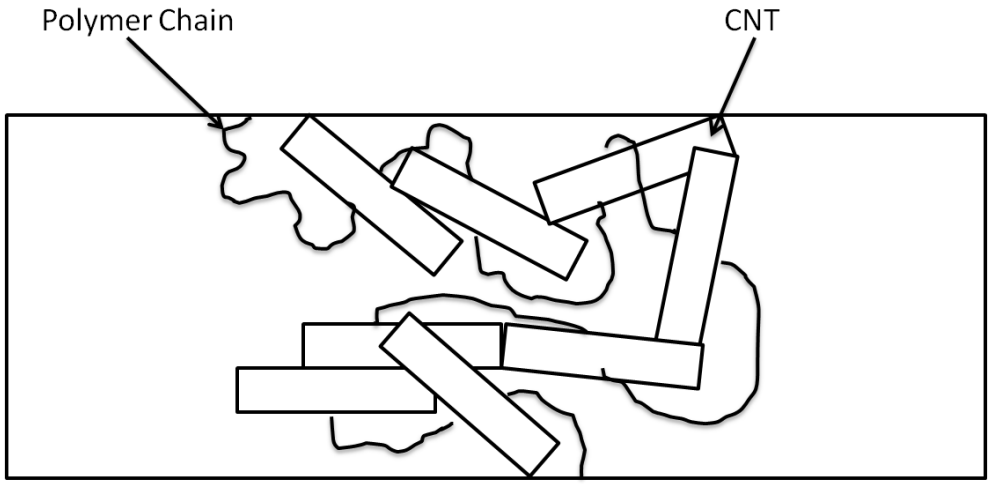

Figure 23. Schematic of Microstructure of Thermal Interface Material Consisting of Polymer with CNTs.

As seen in the figure above, CNTs can align horizontally on top of each other, which is not the ideal orientation for optimal phonon propagation. Researchers have shown huge differences in κ of aligned and un-aligned CNTs[2]. Hone et. al. were able to align carbon nanotubes via a strong magnetic field, as depicted in the figure below.

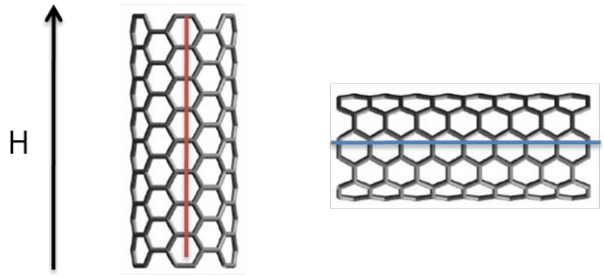

Figure 24. Schematic of H-Alignment of CNT, where H is the Orientation of Magnetic Field (a) Aligned (b) Un-aligned.

They analyzed the effect of CNT orientation (parallel or perpendicular to magnetic field) on κ, as seen below.

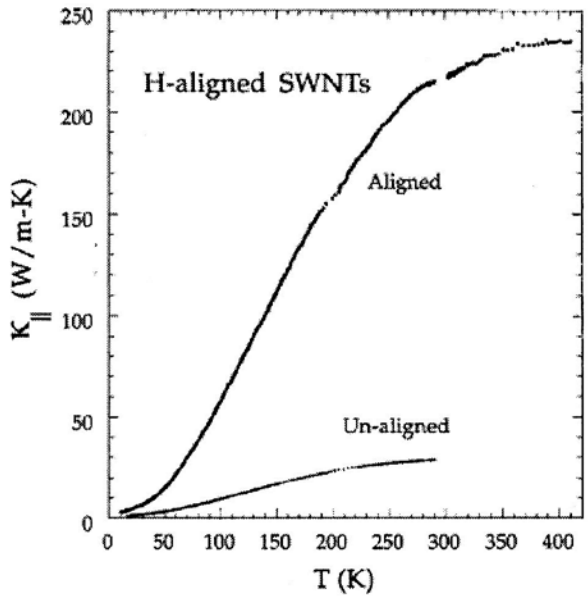

Figure 25. Thermal Conductivity of Aligned and Unaligned SWNTs.[2]

Figure (24) depicts the κ of aligned and un-aligned SWNT. At room temperature there is about a 170 $\frac{W}{mK}$ difference between the κ of aligned and un-aligned CNTs. This effect of orientation may be caused by the variation in contact points based on CNT orientation, as depicted in Figure (23).

The variation in CNT chains within the polymer samples can significantly vary with different sample preparations and could be a cause for the difference in κ of the CNT RET polymer. The interface resistance between the CNT and polymer matrix and/or other CNTs can be very large. This large interface resistance could arise from phonon mismatch of the CNTs and polymer chains[8,2]. The acoustic impedance of a material can be defined as[10]:

$$Z = \rho v \tag{34}$$

where ρ is the mass density and v is the velocity of sound in the material. The velocity term can be defined as[10]:

$$v = \sqrt{\frac{E}{\rho}} \tag{35}$$

where E is the elastic modulus and ρ is the density of the material. Based on Eq. (34) and (35), the acoustic impedance was estimated for CNTs and the RET polymer, 3.24×10^7 and $10\ \left(\frac{Ns}{m^3}\right)$. The transmission coefficient, using Acoustic Mismatch (AMM) model, is defined as[10]:

$$\alpha_{1\to2} = \frac{4Z_1Z_2}{(Z_1+Z_2)^2} \tag{36}$$

Using Eq. (36) an estimated transmission coefficient of 1.23×10^{-6} was obtained. The interface between the CNTs and polymer matrix may enhance phonon scattering

which can result in a drastic reduction of its κ[2,6]. Another possible hypothesis for high interface resistance is a strong coupling between the CNT and polymer chain which may lead to scattering of phonons.

Despite the reasonable calibration results from the reference materials (Stainless Steel and Pyrex) and improvements to the final design, the measured heat flux difference between the meter bars still ranged from 10% - 20%. A possible explanation for this error is that heat is still being lost through conduction through the TCs. A simple experiment was performed on the experimental setup to test this hypothesis. The upper meter bar was replaced with a meter bar with no embedded TCs and tested at the same operating conditions (heater drive voltage, vacuum pressure, and load pressure). Below is a schematic of the experimental setup.

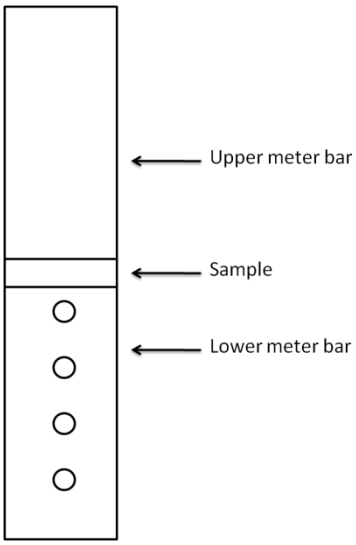

Figure 26. Experimental Setup for Calibration the Possible TC Conduction Loss.

This test will experimentally yield the heat loss due to the TCs (four TCs for the upper meter bar) by comparing the heat flux at the lower meter bar at the standard experimental setup, Figure (14), and the setup mentioned in Figure (25).

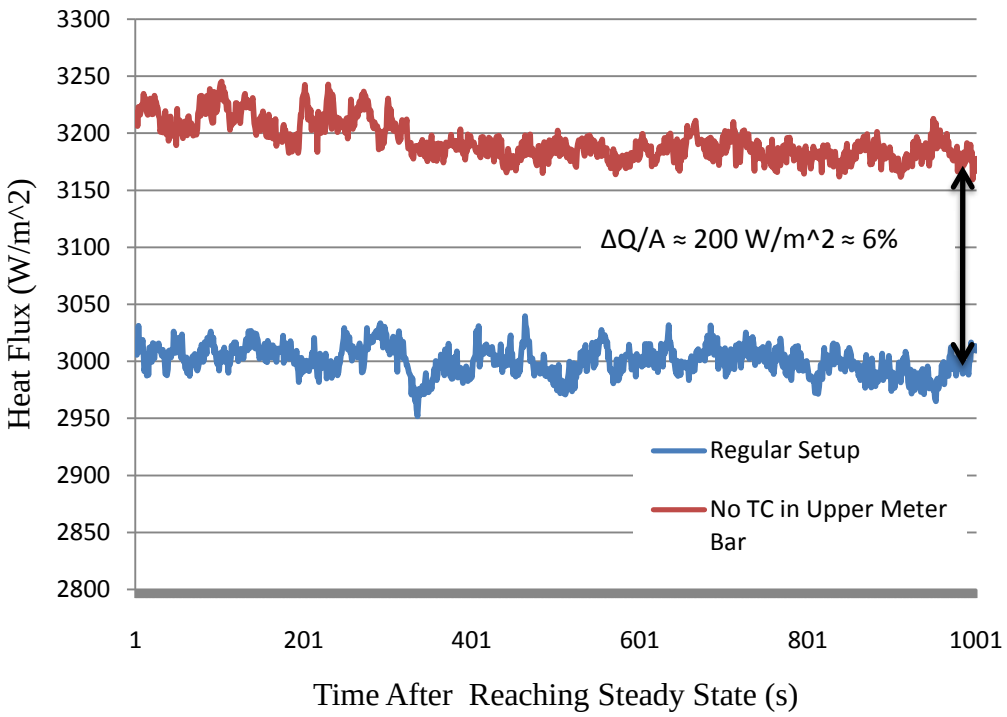

Figure 27. Heat Flux at Lower Meter Bar for Regular and No-Thermocouple Setup.

As seen in the figure above, the heat flux difference experienced by the lower meter bar for the two different experimental setups yielded a difference of 200 $\left(\frac{W}{m^2}\right)$, which equates to about a 6% difference. Based on this result, it was concluded that the four TCs mounted in the upper meter bar resulted in a 200 $\left(\frac{W}{m^2}\right)$ heat loss. Comparing these results with the calculated heat loss from the 22-AWG K-type TC calculated earlier, the heat loss through the TCs is 2.36% of the total heat flowing through the meter bars (~ 0.6 W). If only 2.36% of the heat flux difference is due to conduction losses, the remaining 3.64% could be due to un-accounted heat loss (radiation). To further analyze the effect of TC size on conduction loss, Eq. (2) was utilized to estimate the heat conduction loss for another reduction in TC sizes.

Table 8. Estimated Heat Loss For 22 and 40 AWG K-Type Thermocouples.

Thermocouple Gauge (AWG)	Diameter (m)	Thermal Conductance (W/K)	Heat Loss per Thermocouple (mW)
22	6.50E-04	1.42E-04	3.54
40	8.00E-05	2.14E-06	0.05

As seen in the table above, by reducing the TC size from 22 AWG to 40 AWG, the heat loss per TC decrease 98%.

CONCLUSIONS AND FUTURE WORK:

Steady state thermal measurements depict one possible method to determine the bulk κ of materials. In this thesis, an apparatus designed to measure κ was fabricated based on ASTM D 5470 and ASTM E 1225 standards. To tackle various heat loss mechanisms evident in this thermal conductivity method, many different techniques were utilized.

To eliminate convective effects, the experiment is performed under vacuum. By reducing the operating pressure from atmospheric pressure (~ 760 torr) to ~ 10 millitorr, the h_{conv} is reduced by 10^{-3}. By reducing the diameter of the TCs, heat loss via conduction can be minimized. An ideal TC size would be as small as possible, such as 40 AWG K-type TCs which is estimated to have a heat loss of 0.05 mW per TC. Despite the reduction in conduction heat loss, extremely small TC size, such as 40 AWG, will require special machining to fit holes into the meter bars. Machining mounting holes for the TCs can be a difficult task when drilling small size holes (< 0.6 *mm*) in hard materials/alloys such as stainless steel. It is recommended that TC sizes are chosen based on the smallest available TC size and machining capabilities. Finally, to reduce radiation effects, radiation shields can be implemented. These shields are typically made of extremely low ε values (< 0.05), such as Mylar thermal blankets. By implementing these improvements on the experimental design, the apparatus was able to measure two reference materials (Pyrex and Stainless Steel) within 1% error of their theoretical values. Based on these results, the experimental design was verified and measurements for the unknown CNT RET polymer can now be determined with

reasonable confidence. Thermal conductivity of CNT RET polymer ranging in different volume percentages (1%-20%), were determined via steady state method and compared with 3-ω results. The 3-ω results depict a κ percolation at 5-20% (volume) of CNT and the corresponding κ at this region ranging from ~ 0.45 $\left(\frac{W}{mK}\right)$ to ~ 0.82 $\left(\frac{W}{mK}\right)$. The κ values obtained from steady state methods depicted a linear trend with increasing volume percent. Contrast to the 3-ω values, the κ via steady state method (5%-20% CNT) only ranged from ~ 0.35 $\left(\frac{W}{mK}\right)$ to ~ 0.55 $\left(\frac{W}{mK}\right)$. The differences in κ results could have manifested from variations in the intrinsic test sample configurations. Since functional groups decorate each CNT in a random fashion, each monomer chain (Ethylene, Methyl Methacrylate, and GMA) with CNT attachment could vary significantly. Orientation of the CNTs within the polymer matrix could result in significant changes in κ.

The focus of this thesis was to develop a steady state apparatus that could accurately measure κ. Despite the ability to accurately measure two different reference materials (Pyrex and Stainless Steel), additional improvements to the experimental design could be implemented. Heat loss through radiation and conduction can be an issue in steady state measurements but these effects can be greatly reduced. The distinct heat flux difference between the two reference meter bars are caused by heat loss. As seen in this thesis, radiation effects can make up a significant portion of heat loss. By implementing a heat shield with low emissivity ($\varepsilon \approx 0.03$), the heat flux difference between both meter bars was reduced from 38% down to 16%. Based on ASTM E1225, the heat flux difference between the two meter bars should fall within ~

10%. Heat conduction through the TCs could result in the 16% difference. Theoretical estimates show that the conduction through the TCs make up a 3% difference while experimental results show that the TCs result in a 6% difference. To eliminate heat conduction effects, other researchers (Xu and Fisher) have utilized thermal imaging to monitor the temperature profile of the meter bars[11]. Through this technique Xu and Fisher were able to reduce their heat flux difference between the meter bars to within 6% of each other[11]. To further improve the accuracy and confidence level of the steady state measurements, similar techniques could be implemented to reduce the heat flux difference between the meter bars, which could be around 16% as seen in this thesis. An important aspect in performing steady state thermal conductivity measurements is to reduce the heat flux difference between the meter bars, ultimately reducing heat loss through conduction, convection, and/or radiation, as the key assumption utilized is that heat flux is uniform.

Although CNT based polymers have significant potential in replacing standard SiO_2 TIMs, vertically aligned MWCNT arrays have an even greater potential for future TIMs. One major flaw within polymer based TIMs is that nanotube orientation is inconsistent and ultimately unknown. Utilizing CNT's ability to propagate phonons easily through the tube axis, TIMs of extremely high thermal conductivities can be developed. A major challenge in vertically aligned CNT TIMs is accurately modeling the thermal contact resistance between the substrate and CNT and reducing this contact resistance. Researchers have also investigated the use of additional thermally conductive particles along with CNTs in polymer composites. The use of graphite nanoplatelets (GNPs) and SWCNTs in epoxy composites was reported by Yu et. al. to

have a more efficient percolation and significant reduction in thermal boundary resistance compared to CNT-polymer composites.[2,12] The combination of highly conductive particles coupled with CNTs have great promise for effective TIMs. Further work and research must be devoted to this area in order for CNT TIMs to make its way into future electronic circuits and configurations.

REFERENCES:

[1] Gwinn, J. P., & Webb, R. L. (2003). Performance and Testing of Thermal Interface Materials. *Microelectronics Journal* .

[2] Han, Z., & Fina, A. (2010). Thermal Conductivity of Carbon Nanotubes and their Polymer Nanocomposites: A Review. *Progess in Polymer Science* .

[3] Hone, J., Fischer, J. E., & Walters, D. A. (2000). Electrcial and Thermal Transport Properties of Magnetically Aligned Single Wall Carbon Nanotube Films. *Applied Physics Letters* .

[4] Love, C. T., Xian, G., & Karbhari, V. M. (2007). Thermal, Mechanical, and Adhesive Properties of HDPE/Reactive Ethylene Terpolymer Blends. *Journal of Applied Polymer Science Vol. 104* , 331-338.

[5] Mills, A. F. (1999). *Basic Heat & Mass Transfer.* Upper Saddle River, NJ: Prentice Hall.

[6] Nan, C.-W., Liu, G., Lin, Y., & Li, M. (2004). Interface Effect on Thermal Conductivity of Carbon Nanotube Composites. *Applied Physics Letter Vol. 85* , 3549-3551.

[7] Park, S. H., & Bandaru, P. R. (2010). Improved Mechancial Properties of Carbon Nanotube/Poylmer Composites Through the Use of Carboxyl-Epoxide Functional Group Linkage. *Polymer 51* , 5071-5077.

[8] Prasher, R. (2006). Thermal Interface Materials: Historical Perspective, Status, and Future Directions. *IEEE Vol. 94* , 1571-1586.

[9] Rodriguez, F. (2003). *Principles of Polymer Systems 5th Ed.* NY: Taylor & Francis.

[10] Tritt, T. M. (2004). Measurement Techniques and Considerations for Determining Thermal Conductivity of Bulk Materials. In T. M. Tritt, *Thermal Conductivity Theory, Properities, and Applications.* New York: Plenum Publisher.

[11] Xu, J., & Fisher, T. (2005). Enhancement of Thermal Interface Materials with Carbon Nanotube Arrarus. *Internation Journal of Heat and Mass Transfer* , 1658-1665.

[12] Yu, A., Ramesh, P., & Sun, X. (2008). Enhanced Thermal Conductivity in a Hybrid Graphite Nanoplatelet – Carbon Nanotube Filler for Epoxy Composites. *Advanced Materials* .

[13] Zhu, L., Hess, D. W., & Wong, C. P. (2007). Assembling Carbon Nanotube Films as Thermal Interface Materials. *Electronic Components and Technology Conference* .